APL Materials

Inverse barocaloric effects in ferroelectric $BaTiO_3$ ceramics

Cite as: APL Mater. 4, 091102 (2016); https://doi.org/10.1063/1.4961598
Submitted: 17 June 2016 • Accepted: 11 August 2016 • Published Online: 19 September 2016

E. Stern-Taulats, P. Lloveras, M. Barrio, et al.

Inverse barocaloric effects in ferroelectric $BaTiO_3$ ceramics

E. Stern-Taulats,[1] P. Lloveras,[2] M. Barrio,[2] E. Defay,[3,4] M. Egilmez,[5,a] A. Planes,[1] J.-Ll. Tamarit,[2] Ll. Mañosa,[1] N. D. Mathur,[5] and X. Moya[5,b]
[1]*Facultat de Física, Departament de Física de la Matèria Condensada, Universitat de Barcelona, Martí i Franquès 1, Barcelona 08028, Catalonia, Spain*
[2]*Departament de Física, ETSEIB, Universitat Politècnica de Catalunya, Diagonal 647, Barcelona 08028, Catalonia, Spain*
[3]*CEA, LETI, Minatec Campus, 17 Rue des Martyrs, Grenoble 38054, France*
[4]*Materials Research and Technology Department, Luxembourg Institute of Science and Technology (LIST), 41 rue du Brill, Belvaux L-4422, Luxembourg*
[5]*Department of Materials Science, University of Cambridge, Cambridge CB3 0FS, United Kingdom*

(Received 17 June 2016; accepted 11 August 2016; published online 19 September 2016)

We use calorimetry to identify pressure-driven isothermal entropy changes in ceramic samples of the prototypical ferroelectric $BaTiO_3$. Near the structural phase transitions at ~400 K (cubic-tetragonal) and ~280 K (tetragonal-orthorhombic), the inverse barocaloric response differs in sign and magnitude from the corresponding conventional electrocaloric response. The differences in sign arise due to the decrease in unit-cell volume on heating through the transitions, whereas the differences in magnitude arise due to the large volumetric thermal expansion on either side of the transitions. [http://dx.doi.org/10.1063/1.4961598]

The discovery one decade ago of giant electrocaloric (EC) effects near ferroelectric phase transitions in ceramic thin films,[1] and then in thicker films of polymers,[2] triggered intense research into ferroelectric materials for environmentally friendly EC cooling.[3–6] Although there have been significant advances in materials developments,[7–9] measuring techniques,[10–16] and heat-pump prototypes,[17–21] the commercial application of EC materials remains elusive. The main obstacle is that EC performance is limited by breakdown field, while another major obstacle is that electric-field-induced strain produces mechanical fatigue and ultimately failure. This second obstacle arises because the ferroelectric phase transitions exploited in EC effects are typically accompanied by significant changes in volume.[22–24] It therefore follows that EC materials are good candidates for solid-state barocaloric (BC) cooling.[5,6,25]

BC effects are reversible thermal changes driven by changes of hydrostatic pressure and have long been exploited in fluids to achieve continuous cooling in the well known vapour-compression systems employed in refrigerators and air conditioners. Given that these BC fluids are harmful for the environment, it would be attractive to replace them with non-volatile materials that show large BC effects. Large BC effects have recently been predicted in two ferroelectric materials [$PbTiO_3$ and $BaTiO_3$ (BTO)[26,27]] and experimentally demonstrated in ferrielectric ammonium sulphate.[28] Moreover, it is easier to exploit ferroelectric materials for BC cooling than EC cooling, as there is no need to fabricate multilayer capacitor devices for electrical access to films; there is no mechanical fatigue/failure during operation; and the range of operating temperatures is not compromised by the need to avoid breakdown.[5,6,28]

[a]Present address: Department of Physics, American University of Sharjah, Sharjah 26666, United Arab Emirates.
[b]Author to whom correspondence should be addressed. Electronic mail: xm212@cam.ac.uk

Here we use temperature-dependent x-ray diffraction, and pressure-dependent calorimetry, to experimentally demonstrate BC effects in ceramics of the prototypical ferroelectric BTO. The combination of these two techniques is essential for evaluating contributions to the BC response that arise from the non-isochoric phase transitions and the volumetric thermal expansion on either side of each transition.[28] At high temperatures, BTO displays a centrosymmetric cubic ABO_3 perovskite structure, with A cations at the corners, B cations at the centres, and oxygen anions at the face-centred positions. Near the transition between cubic (C) and tetragonal (T) phases[22,23] at Curie temperature $T_C \sim 400$ K, we find inverse isothermal entropy changes of magnitude $|\Delta S| \sim 1.6$ J K^{-1} kg^{-1} due to small changes of applied pressure $|\Delta p| \sim 1$ kbar (assuming ambient pressure to be zero, such that $|\Delta p| \sim p$). At lower temperatures, near the ~280 K transition between T and orthorhombic (O) phases, we find inverse isothermal entropy changes of magnitude $|\Delta S| \sim 1.3$ J K^{-1} kg^{-1}, also with $|\Delta p| \sim 1$ kbar. We did not explore the ~200 K transition between O and rhombohedral (R) phases, as the change in unit-cell volume is small [Figure S1 of the supplementary material].

Powdered BTO (≥99.99%) from Sigma-Aldrich had a typical grain size of <1 μm. The powder was first cold-pressed isostatically in air at 10 kbar and then sintered in air at 1673 K for 48 h. The sintered ceramic (2.3 cm in diameter, 0.2 cm in thickness) was cooled down to room temperature at −3 K min^{-1}. A small piece (~0.005 cm^3) was cut in order to perform temperature-dependent calorimetry and x-ray diffraction at ambient pressure. The larger remaining piece was used for pressure-dependent calorimetry.

Measurements of dQ/dT at atmospheric pressure were performed using a commercial TA Q2000 differential scanning calorimeter at ±2 K min^{-1} (Q is heat, T is temperature). Heat $|Q_0| = \left|\int_{T_1}^{T_2}(dQ/dT')\,dT'\right|$ and entropy change $|\Delta S_0| = \left|\int_{T_1}^{T_2}(dQ/dT')/T'\,dT'\right|$ across the first-order transitions were obtained after subtracting baseline backgrounds,[29] with T_1 chosen above (below) each transition on cooling (heating), and T_2 chosen below (above) each transition on cooling (heating). The entropy change on partially driving each transition by heating to temperature T, with respect to each low-temperature phase, is $\Delta S(T) = \int_{T_1}^{T}(dQ/dT')/T'\,dT'$. The entropy change on partially driving each transition by cooling to temperature T, with respect to each low-temperature phase, is $\Delta S(T) = |\Delta S_0| - \int_{T_1}^{T}(dQ/dT')/T'\,dT'$.

High-resolution x-ray diffraction was performed in transmission-mode using Cu $K\alpha_1 = 1.5406$ Å radiation in an INEL diffractometer, with a curved position-sensitive detector (CPS120), and Debye-Scherrer geometry. The sample was introduced into a 0.3-mm diameter Lindemann capillary to minimise absorption, and temperature was varied using a liquid-nitrogen 700 series Oxford Cryostream Cooler. Lattice parameters were determined by pattern matching using FullProf software.[30]

Measurements of dQ/dT under hydrostatic pressure were performed at approximately ±2 K min^{-1}, using a differential thermal analyser constructed in-house. At high temperatures, we used an Irimo Bridgman pressure cell that operates at up to 3 kbar and a resistive heater (room temperature-473 K). At low temperatures, we used a Cu-Be Bridgman pressure cell that operates at up to 3 kbar and a circulating thermal bath (Lauda Proline RP 1290, 183-473 K). In order to guarantee optimal thermal contact between the heat sensor and the sample, a chromel-alumel thermocouple was inserted inside a hole that was drilled in the centre of the large BTO ceramic sample. The ceramic sample and thermocouple were then immersed in the pressure-transmitting medium (Caldic silicon oil for high-temperature measurements; DW-Therm, Huber Kältemaschinenbau GmbH for low-temperature measurements).

The first-order structural phase transitions are seen in calorimetry [Figure 1(a)] to be sharp, with a small thermal hysteresis of ~4 K (C-T) and ~7 K (T-O). Integration of $(dQ/dT)/T$ yields the thermally driven entropy change $\Delta S(T)$ [Figure 1(b)], with $|\Delta S_0| = 2.4 \pm 0.2$ J K^{-1} kg^{-1} for the full C-T transition and $|\Delta S_0| = 2.0 \pm 0.2$ J K^{-1} kg^{-1} for the full T-O transition. Integration of dQ/dT across the full transition yields heats of $|Q_0| = 960 \pm 90$ J kg^{-1} (C-T) and $|Q_0| = 560 \pm 60$ J kg^{-1} (T-O). These values are in good agreement with previous experimental values[12,31] of $|\Delta S_0| \sim 2.4$ J K^{-1} kg^{-1} and $|Q_0| \sim 900$ J kg^{-1} for the C-T transition and are similar to previous values[31,32] of $|\Delta S_0| \sim 1.6$-2.3 J K^{-1} kg^{-1} and $|Q_0| \sim 450$-640 J kg^{-1} for the T-O transition.

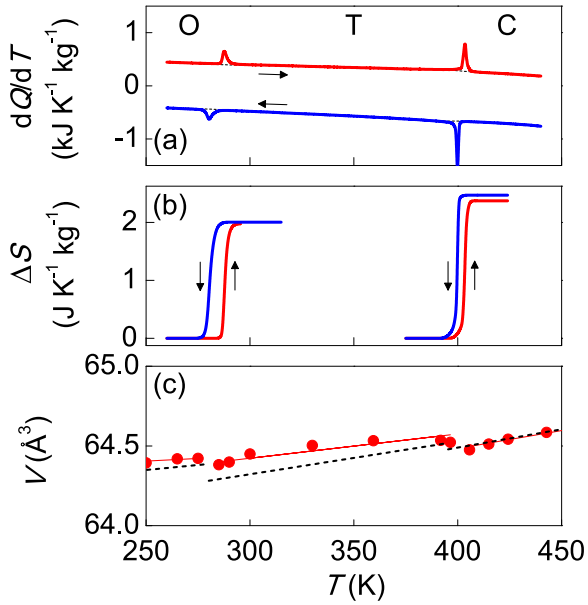

FIG. 1. Structural phase transitions in BTO at ambient pressure. (a) dQ/dT on cooling (blue) and heating (red) across the cubic-tetragonal (C-T) and tetragonal-orthorhombic (T-O) transitions. Baselines are black dotted lines, and $dQ/dT > 0$ denotes endothermic processes. (b) Entropy change $\Delta S(T)$ with respect to the low-temperature phase for each transition. Arrows in (a) and (b) show direction of temperature sweep. (c) Unit-cell volume $V(T)$ on heating. Selected diffraction patterns are shown in Figure S2 of the supplementary material; temperature-dependent lattice parameters are shown in Figure S3 of the supplementary material. Solid lines represent linear fits. Dashed lines represent the literature data.[22,23]

On heating through the two transitions, x-ray diffraction data [Figure 1(c)] confirm the expected changes in crystal structure.[22,23] The unit-cell volume V decreases sharply by ~0.03% (O-T transition, $\Delta V_0 = -0.02 \pm 0.01$ Å^3) and ~0.11% (T-C, $\Delta V_0 = -0.07 \pm 0.02$ Å^3). On either side of each transition, the volume thermal expansion is large [Figure S1 of the supplementary material], implying large additional BC effects.[28] By writing isothermal BC entropy change per unit mass m due to pressure change $\Delta p = p_2 - p_1$ as[5,28] $\Delta S(p_1 \rightarrow p_2) = -m^{-1} \int_{p_1}^{p_2} (\partial V/\partial T)_{p'} dp'$ (using the Maxwell relation $m^{-1}(\partial V/\partial T)_p = -(\partial S/\partial p)_T$), we therefore anticipate inverse BC effects in the transition regimes where $(\partial V/\partial T)_{p=0} < 0$, and conventional BC effects outside the transition regimes where $(\partial V/\partial T)_{p=0} > 0$.

dQ/dT measurements through the two transitions under various applied pressures are shown in Figure 2. For the C-T transition, there is a strong pressure-induced shift of transition temperature T_0, with $dT_0/dp = -5.8 \pm 0.1$ K kbar^{-1} on heating and $dT_0/dp = -5.4 \pm 0.2$ K kbar^{-1} on cooling [Figures 2(a) and 2(c)]. A larger shift of -7.9 ± 2.0 K kbar^{-1} on heating is obtained via the Clausius-Clapeyron equation $dT_0/dp = \Delta v_0/\Delta S_0$, using $\Delta S_0 = 2.4 \pm 0.2$ J K^{-1} kg^{-1} [Figure 1(b)] and specific volume change $\Delta v_0 = -(0.19 \pm 0.03) \times 10^{-6}$ m^3 kg^{-1} [from Figure 1(c)]. These values of dT_0/dp are similar to those reported for BTO in the form of single crystals (~−4-6 K kbar^{-1}, Refs. 33–40) and ceramics (~−4-5 K kbar^{-1}, Refs. 36, 40, and 41), and they imply that the narrow first-order transition of width ~4 K may be fully driven using low values of $|\Delta p| \sim 1$ kbar.

For the T-O transition, the pressure-induced shift in T_0 is weaker, with $dT_0/dp = -3.5 \pm 0.1$ K kbar^{-1} on heating and $dT_0/dp = -2.6 \pm 0.1$ K kbar^{-1} on cooling [Figures 2(b) and 2(c)]. A similar shift of $dT_0/dp = -2.8 \pm 1.3$ K kbar^{-1} on heating is obtained via the Clausius-Clapeyron equation, using $\Delta S_0 = 2.0 \pm 0.2$ J K^{-1} kg^{-1} [Figure 1(b)] and specific volume change $\Delta v_0 = -(0.06 \pm 0.03) \times 10^{-6}$ m^3 kg^{-1} [from Figure 1(c)]. These values of dT_0/dp are similar to those reported for single-crystal BTO (~−3 K kbar^{-1}, Refs. 35, 37, 40, and 42) and indicate that the wider first-order transition of width ~7 K may be fully driven using $|\Delta p| \sim 2$ kbar.

For each of the two transitions, integration of $(dQ/dT)/T$ at finite pressure reveals that the entropy change $|\Delta S_0|$ decreases with increasing pressure [Figure 2(d)]. This fall in $|\Delta S_0|$ arises because of

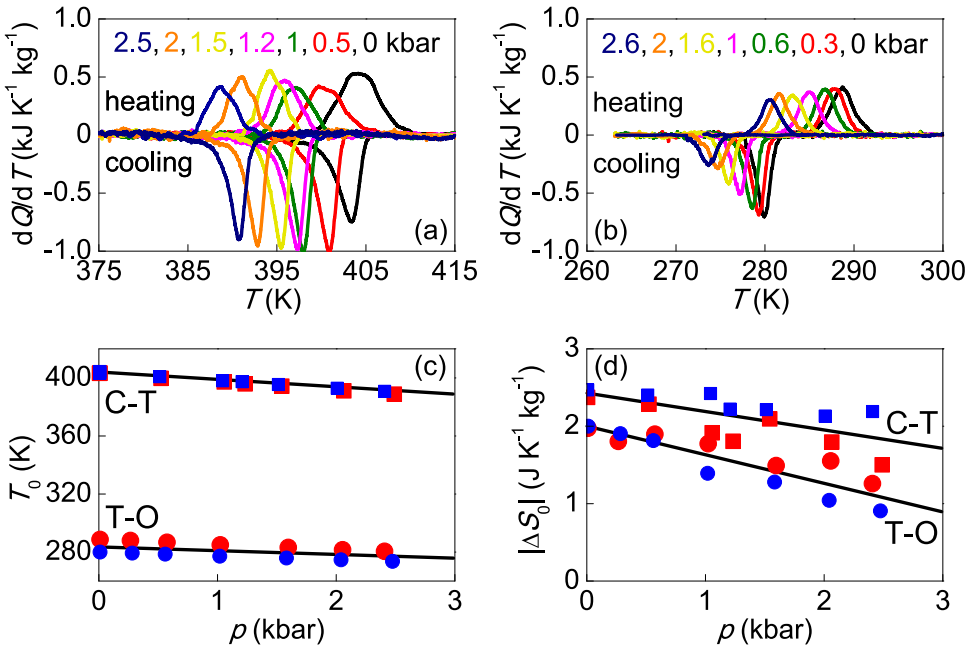

FIG. 2. Structural phase transitions in BTO under pressure. dQ/dT on cooling and heating across (a) the C-T and (b) T-O transitions, after baseline subtraction, for different values of increasing pressure p, values of which appear in the same order as the peaks for both heating and cooling. Pressure dependence of (c) transition temperature T_0 and (d) entropy change $|\Delta S_0|$, for the C-T transition [square symbols, data from (a)] and the T-O transition [round symbols, data from (b)] on cooling (small blue symbols) and heating (large red symbols). Lines in (c) and (d) are linear fits.

additional[28] changes in isothermal entropy $\Delta S_+(p)$ that are conventional, reversible, and opposite in sign with respect to the pressure-driven isothermal entropy changes associated with each transition. These additional changes in entropy are challenging to detect via the calorimetry used for Figure 2 but may be expressed away from the first-order transitions via $\Delta S_+(p) = -[m^{-1}(\partial V/\partial T)_{p=0}]p$, where we have used the aforementioned Maxwell relation with S_+ replacing S, and with $(\partial V/\partial T)_p$ assumed independent of pressure.[5,28]

In order to plot $\Delta S(T,p)$ with respect to the zero-pressure entropy at a temperature T_+ above the C-T transition [Figures 3(a) and 3(b)] and the T-O transition [Figures 4(a) and 4(b)], we obtained finite-pressure plots of $\Delta S(T)$ [from the integration of data in Figures 2(a) and 2(b)] that we displaced[28] at T_+ by evaluating $\Delta S_+(p)$ at this temperature. Note that $\Delta S_+(p)$ was evaluated at $T_+ > T_0(p)$ to avoid the forbidden possibility of $T_0(p)$ falling to T_+ at high pressure.

For the C-T transition, our plots in Figure 3(a) of $\Delta S(T,p)$ for dQ/dT data obtained on heating permit us to establish isothermal BC effects on applying pressure [Figure 3(c)], as heating and high pressure both favour the high-temperature cubic phase with smaller volume. Similarly, our plots in Figure 3(b) of $\Delta S(T,p)$ for dQ/dT data obtained on cooling permit us to establish isothermal BC effects on decreasing pressure [Figure 3(d)], as cooling and low pressure both tend to favour the low-temperature tetragonal phase with larger volume. Values of $|\Delta S(T,p)|$ on applying and removing pressure are similar at all temperatures studied. The BC response near the C-T transition is therefore highly reversible, consistent with the low thermal hysteresis of the transition [Figures 1(a) and 1(b)]. The peak isothermal entropy change $|\Delta S| \sim 1.6 \pm 0.2$ J K^{-1} kg^{-1} near ~400 K is achieved with a low value of $|\Delta p| = 1$ kbar [Figures 3(c) and 3(d)], yielding large BC strengths,[5] $|\Delta S|/|\Delta p|$ and $|Q|/|\Delta p|$ (Table I). Larger pressures extend inverse reversible BC effects to lower temperatures, causing an increase of refrigerant capacity RC [Figure 5(b)], despite the reduction in $|\Delta S_0(p)|$ [Figure 2(d)] and thus the peak value of $|\Delta S(p)|$ [Figure 5(a)]. Note that recently predicted BC effects ($|\Delta S| \sim 3.9$ J K^{-1} kg^{-1} with 10 kbar at 353 K) are larger because additional entropy changes were neglected.[27]

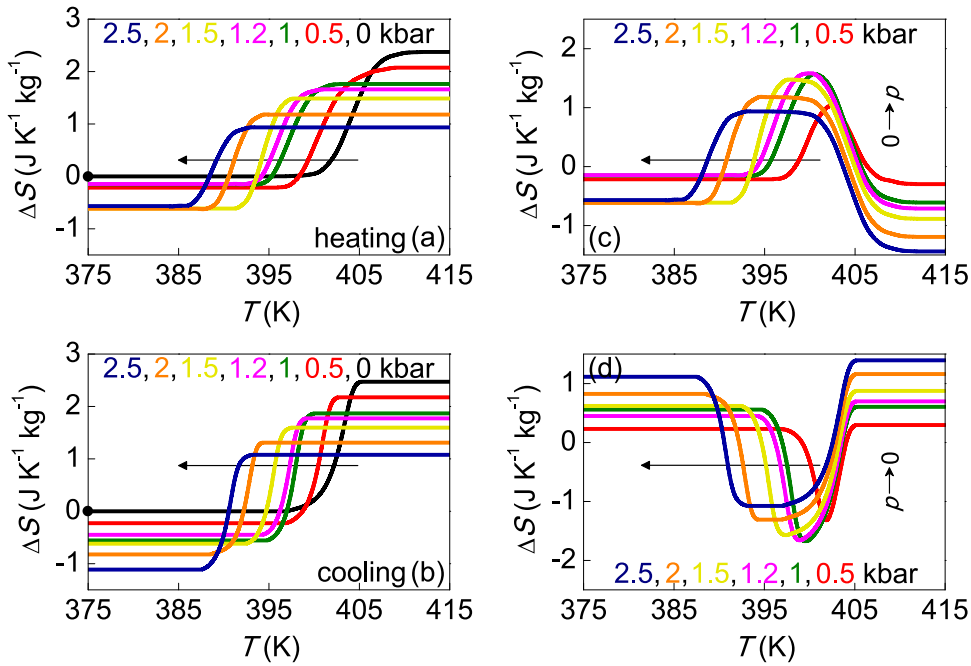

FIG. 3. Inverse barocaloric effects in BTO near the C-T phase transition. For (a) heating and (b) cooling, we show entropy change $\Delta S(T, p)$ with respect to $S(T = 375\ \text{K}, p = 0)$ (black dot), offsetting $\Delta S(T)$ at each pressure using additional entropy change $\Delta S_+(p)$ at $T_+ = 410$ K. Hence isothermal entropy change $\Delta S(p)$ for (c) increasing pressure $(0 \rightarrow p)$ as deduced from (a), and (d) decreasing pressure $(p \rightarrow 0)$ as deduced from (b). In each panel, the given pressure values increase as indicated by the horizontal arrow.

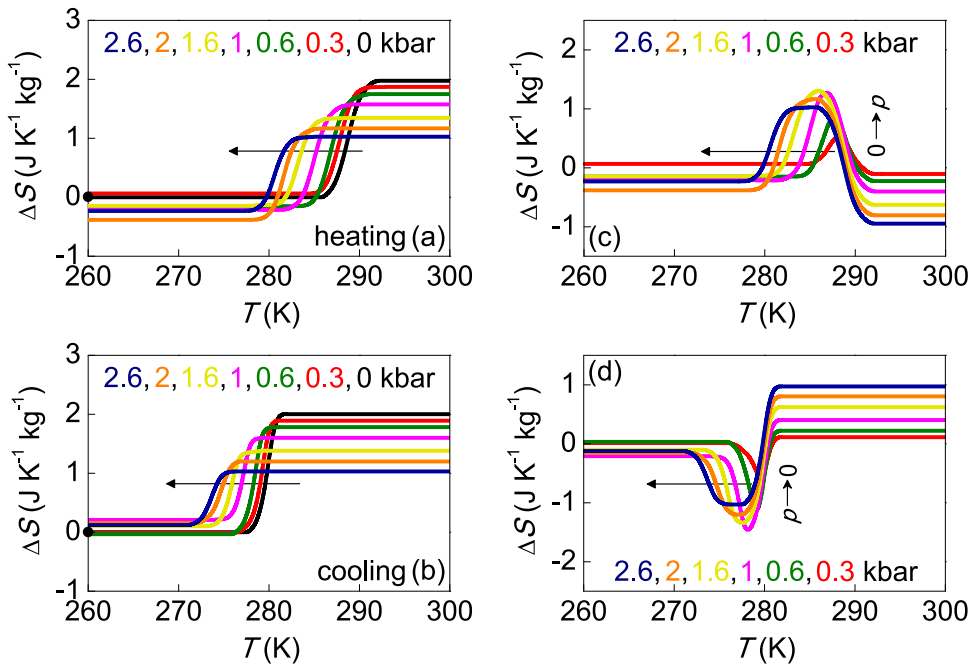

FIG. 4. Inverse barocaloric effects in BTO near the T-O phase transition. For (a) heating and (b) cooling, we show entropy change $\Delta S(T, p)$ with respect to $S(T = 260\ \text{K}, p = 0)$ (black dot), offsetting $\Delta S(T)$ at each pressure using additional entropy change $\Delta S_+(p)$ at $T_+ = 292$ K for (a), and at $T_+ = 282$ K for (b). Hence isothermal entropy change $\Delta S(p)$ for (c) increasing pressure $(0 \rightarrow p)$ as deduced from (a), and (d) decreasing pressure $(p \rightarrow 0)$ as deduced from (b). In each panel, the given pressure values increase as indicated by the horizontal arrow.

TABLE I. Comparison of inverse barocaloric effects and conventional electrocaloric effects in BTO. Isothermal entropy change ΔS and isothermal heat Q, at starting temperature T, due to changes of hydrostatic pressure Δp, and changes of electric field ΔE. The corresponding strengths are $|\Delta S|/|\Delta p| = 1.6$ J K^{-1} kg^{-1} kbar^{-1} and $|Q|/|\Delta p| = 660$ J kg^{-1} kbar^{-1} for the C-T transition, and $|\Delta S|/|\Delta p| = 1.3$ J K^{-1} kg^{-1} kbar^{-1} and $|Q|/|\Delta p| = 365$ J kg^{-1} kbar^{-1} for the T-O transition. For ΔS and Q, bold entries denote data derived from direct measurements, other entries denote data derived from quasi-direct[5] measurements. For all entries, $Q = T\Delta S$.

Transition	T (K)	Caloric effect	Single crystal or Polycrystal	ΔS (J K^{-1} kg^{-1})	Q (J kg^{-1})	Δp or ΔE	References
C-T	400	BC	Polycrystal	1.6	660	1 kbar	This work
		EC	Single crystal	**−2.1**	**−840**	4 kV cm^{-1}	12
T-O	280	BC	Polycrystal	1.3	365	1 kbar	This work
		EC	Single crystal	**−2.3**	**−645**	10 kV cm^{-1}	43

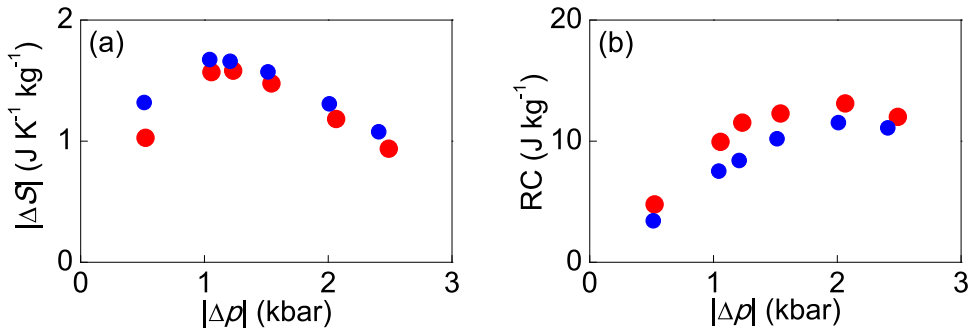

FIG. 5. Peak BC response and refrigerant capacity near the C-T phase transition. (a) Peak values $|\Delta S|$ of the temperature-dependent entropy change $\Delta S(T)$ at each measurement pressure p, for applying pressure (large red symbols) and removing pressure (small blue symbols). (b) The corresponding refrigerant capacity RC = $|\Delta S| \times$ [FWHM of $\Delta S(T)$] for selected pressure changes of magnitude $|\Delta p| \sim |p|$.

For the T-O transition, our plots in Figures 4(a) and 4(b) of $\Delta S(T,p)$ for dQ/dT data obtained on heating and cooling permit us to establish isothermal BC effects on increasing pressure [Figure 4(c)] and decreasing pressure [Figure 4(d)]. Although the peak entropy change of $|\Delta S| \sim 1.3 \pm 0.2$ J K^{-1} kg^{-1} appears to be similar for $\Delta p = \pm 1$ kbar, the peak occurs at different temperatures, evidencing inverse irreversible BC effects. This irreversibility, which is also seen for conventional EC effects near the T-O transition,[43] arises because of the relatively large thermal hysteresis. Therefore caloric effects near the T-O transition are unsuitable for continuous cooling, and so we do not present RC values.

In summary, we have combined temperature-dependent x-ray diffraction data with pressure-dependent calorimetry to demonstrate BC effects in BTO ceramic samples. For the T-O phase transition at ~280 K, we found small inverse BC effects that are irreversible, whereas for the C-T phase transition at Curie temperature $T_C \sim 400$ K, we found larger inverse BC effects that are reversible. Our observation of reversible BC effects near the Curie temperature of BTO should inspire studies of BC effects in a wide range of ferroelectric materials. This should expand the range of BC materials beyond ammonium sulphate[28] and a small number of magnetic materials,[44–48] allowing caloric properties to be exploited in cooling devices without the electrical breakdown that limits EC effects.

See supplementary material for Figures S1, S2, and S3. All relevant data are presented via this publication and supplementary material.

This work was supported by the ERC Starting Grant No. 680032, the UK EPSRC Grant No. EP/M003752/1, by CICyT (Spain), Project Nos. MAT2013-40590-P and FIS2014-54734-P, and by DGU (Catalonia), Project No. 2014SGR00581. P.Ll. acknowledges support from SUR (DEC,

Catalonia). E.S.T. acknowledges support from AGAUR. E.D. acknowledges support from FNR Luxembourg through COFERMAT project. X.M. is grateful for support from the Royal Society.

[1] A. S. Mischenko, Q. Zhang, J. F. Scott, R. W. Whatmore, and N. D. Mathur, Science **311**, 1270 (2006).
[2] B. Neese, B. Chu, S.-G. Lu, Y. Wang, E. Furman, and Q. M. Zhang, Science **321**, 821 (2008).
[3] J. F. Scott, Annu. Rev. Mater. Res. **41**, 229 (2011).
[4] M. Valant, Prog. Mater. Sci. **57**, 980 (2012).
[5] X. Moya, S. Kar-Narayan, and N. D. Mathur, Nat. Mater. **13**, 439 (2014).
[6] S. Crossley, N. D. Mathur, and X. Moya, AIP Adv. **5**, 067153 (2015).
[7] X.-S. Qian, S.-G. Lu, X. Li, H. Gu, L.-C. Chien, and Q. Zhang, Adv. Funct. Mater. **23**, 2894 (2013).
[8] Q. Li, G. Zhang, X. Zhang, S. Jiang, Y. Zeng, and Q. Wang, Adv. Mater. **27**, 2236 (2015).
[9] G. Zhang, X. Zhang, T. Yang, Q. Li, L.-Q. Chen, S. Jiang, and Q. Wang, ACS Nano **9**, 7164 (2015).
[10] S. G. Lu, B. Rožič, Q. M. Zhang, Z. Kutnjak, and B. Neese, Appl. Phys. Lett. **98**, 122906 (2011).
[11] F. Le Goupil, A. Berenov, A.-K. Axelsson, M. Valant, and N. McN. Alford, J. Appl. Phys. **111**, 124109 (2012).
[12] X. Moya, E. Stern-Taulats, S. Crossley, D. González-Alonso, S. Kar-Narayan, A. Planes, Ll. Mañosa, and N. D. Mathur, Adv. Mater. **25**, 1360 (2013).
[13] S. Kar-Narayan, S. Crossley, X. Moya, V. Kovacova, J. Abergel, A. Bontempi, N. Baier, E. Defay, and N. D. Mathur, Appl. Phys. Lett. **102**, 032903 (2013).
[14] Y. Jia and Y.-S. Ju, Appl. Phys. Lett. **103**, 042903 (2013).
[15] D. Guo, J. Gao, Y.-J. Yu, S. Santhanam, G. K. Fedder, A. J. H. McGaughey, and S. C. Yao, Appl. Phys. Lett. **105**, 031906 (2014).
[16] T. Tong, J. Karthik, R. V. K. Mangalam, L. W. Martin, and D. G. Cahill, Phys. Rev. B **90**, 094116 (2014).
[17] Y. Jia and Y.-S. Ju, Appl. Phys. Lett. **100**, 242901 (2012).
[18] H. Gu, X. Qian, X. Li, B. Craven, W. Zhu, A. Cheng, S. C. Yao, and Q. M. Zhang, Appl. Phys. Lett. **102**, 122904 (2013).
[19] H. Gu, X.-S. Qian, H.-J. Ye, and Q. M. Zhang, Appl. Phys. Lett. **105**, 162905 (2014).
[20] U. Plaznik, A. Kitanovski, B. Rožič, B. Malič, H. Ursič, S. Drnovšek, J. Cilenšek, M. Vrabelj, A. Poredoš, and Z. Kutnjak, Appl. Phys. Lett. **106**, 043903 (2015).
[21] S. J. Smullin, Y. Wang, and D. E. Schwartz, Appl. Phys. Lett. **107**, 093903 (2015).
[22] H. F. Kay and P. Vousden, London Edinburgh Dublin Philos. Mag. J. Sci. **40**, 1019 (1949).
[23] G. H. Kwei, A. C. Lawson, S. J. L. Billinge, and S.-W. Cheong, J. Phys. Chem. **97**, 2368 (1993).
[24] G. Shirane, S. Hoshino, and K. Suzuki, Phys. Rev. **80**, 1105 (1950).
[25] Ll. Mañosa, A. Planes, and M. Acet, J. Mater. Chem. A **1**, 4925 (2013).
[26] E. A. Mikhaleva, I. N. Flerov, M. V. Gorev, M. S. Molokeev, A. V. Cherepakhin, A. V. Kartashev, N. V. Mikhashenok, and K. A. Sablina, Phys. Solid State **54**, 1832 (2012).
[27] Y. Liu, J. Wei, P.-E. Janolin, I. C. Infante, X. Lou, and B. Dkhil, Appl. Phys. Lett. **104**, 162904 (2014).
[28] P. Lloveras, E. Stern-Taulats, M. Barrio, J.-Ll. Tamarit, S. Crossley, W. Li, V. Pomjakushin, A. Planes, Ll. Mañosa, N. D. Mathur, and X. Moya, Nat. Commun. **6**, 8801 (2015).
[29] J. Ortín and A. Planes, Acta Metall. **36**, 1873–1889 (1988).
[30] J. Rodriguez, T. Roisnel, and P. J. Gonzales, *FullProf Suite* (Laboratoire Leon Brillouin, CEA-CNRS, CEN Saclay, France, 2005).
[31] G. Shirane, H. Danner, A. Pavlovic, and R. Pepinsky, Phys. Rev. **93**, 672 (1954).
[32] X. Moya, L. E. Hueso, F. Maccherozzi, A. I. Tovstolytkin, D. I. Podyalovskii, C. Ducati, L. C. Phillips, M. Ghidini, O. Hovorka, A. Berger, M. E. Vickers, E. Defay, S. S. Dhesi, and N. D. Mathur, Nat. Mater. **12**, 52 (2013).
[33] W. J. Merz, Phys. Rev. **77**, 52 (1950).
[34] J. Klimowski, Phys. Status Solidi **2**, 456 (1962).
[35] S. Minomura, T. Kawakubo, T. Nakagawa, and S. Sawada, Jpn. J. Appl. Phys. **3**, 562 (1964).
[36] G. A. Samara, Phys. Rev. **151**, 378 (1966).
[37] G. A. Samara, Ferroelectrics **2**, 277 (1971).
[38] R. Clarke and L. Benguigui, J. Phys. C: Solid State Phys. **10**, 1963 (1977).
[39] M. Malinowski, K. Lukaszewicz, and S. Asbrink, J. Appl. Crystallogr. **19**, 7 (1986).
[40] T. Ishidate, S. Abe, H. Takahashi, and N. Môri, Phys. Rev. Lett. **78**, 2397 (1997).
[41] J. L. Zhu, S. Lin, S. M. Feng, F. Y. Li, L. J. Wang, C. Q. Jin, X. H. Wang, and L. T. Li, J. Phys.: Conf. Ser. **121**, 162005 (2008).
[42] S. Minomura, M. Tanaka, B. Okai, and H. Nagasaki, J. Phys. Soc. Jpn. **28**(Suppl.), 404 (1970).
[43] Y. Bai, K. Ding, G.-P. Zheng, S.-Q. Shi, J.-L. Cao, and L. Qiao, AIP Adv. **2**, 022162 (2012).
[44] Ll. Mañosa, D. González-Alonso, A. Planes, E. Bonnot, M. Barrio, J.-Ll. Tamarit, S. Aksoy, and M. Acet, Nat. Mater. **9**, 478 (2010).
[45] S. Yuce, M. Barrio, B. Emre, E. Stern-Taulats, A. Planes, J.-Ll. Tamarit, Y. Mudryk, K. A. Gschneidner, Jr., V. K. Pecharsky, and Ll. Mañosa, Appl. Phys. Lett. **101**, 071906 (2012).
[46] Ll. Mañosa, D. González-Alonso, A. Planes, M. Barrio, J.-Ll. Tamarit, I. S. Titov, M. Acet, A. Bhattacharyya, and S. Majumdar, Nat. Commun. **2**, 595 (2011).
[47] E. Stern-Taulats, A. Planes, P. Lloveras, M. Barrio, J.-Ll. Tamarit, S. Pramanick, S. Majumdar, C. Frontera, and Ll. Mañosa, Phys. Rev. B **89**, 214105 (2014).
[48] D. Matsunami, A. Fujita, K. Takenaka, and M. Kano, Nat. Mater. **14**, 73 (2014).